Detection of Areas Associated with Flood and Erosion Caused by a Heavy Rainfall Using Multitemporal Landsat TM Data

Amod Sagar Dhakal, Takaaki Amada, Masamu Aniya, and Rishi Ram Sharma

Abstract

The potential of multitemporal Landsat Thematic Mapper (TM) data was examined for its use in detecting areas affected by flood and erosion from a heavy rainfall. The study area is the Kulekhani watershed (124 km^2) located in the central region of Nepal. Four change-detection techniques were compared for their effectiveness including (1) Spectral Image Differencing (SID), (2) Tasseled Cap Brightness Image Differencing (TCBID), (3) Principal Component Analysis (PCA), and (4) Spectral Change Vector Analysis (SCVA). SID was performed on four raw bands (bands 1, 2, 3, and 7), and altogether seven new images (change images) were produced.

Visible bands were effective in detecting affected areas. SCVA (using bands 1, 2, and 3) was found to be most accurate for detecting areas affected by flood and erosion followed by SID (band 2), PCA (using bands 1, 2, and 3), SID (band 1), and SID (band 3). The change image produced from SCVA showed overall and Khat accuracies of 88.3 percent and 75.4 percent, respectively. The analysis of spatial agreement conducted among the seven change images, produced from different techniques, varied from 89 percent to 98 percent. The change image produced from SCVA showed high spatial agreements with change images produced from PCA, SID (band 3), and SID (band 2). SCVA and SID (band 3) showed the spatial agreement of 88.1 percent and 98.7 percent in the change and no-change categories, respectively.

Introduction

High precipitation often causes sediment-related phenomena such as landslides, debris flows, flash floods, and floods, posing significant hazards to humans and property. The detection of areas associated with such disturbances for a large area is critical for the assessment of and the response to disturbances at medium or smaller scale hazard evaluations (Cuny, 1983; Kienholz *et al.*, 1984; ICIMOD 1991; Cablik *et al.* 1994; Dhakal *et al.*, 2000; Zhou *et al.*, 2000). For large areas, mapping of affected sites from a field survey is complicated, time consuming, and costly (Aniya *et al.*, 1985; Sakai *et al.*, 1985). Although conventional aerial photographs remain an important remote sensing means for accurate mapping of such areas, they have disadvantages in that a large number of photographs are required for the analysis (e.g., Brabb, 1991), and mapping is largely dependent on the experience of the analyst (Fookes *et al.*, 1991; Carrara *et al.*, 1992; Van westen 1993; Carrara *et al.*, 1995; Mantovani *et al.*, 1996; Dhakal *et al.*, 1999). Often the utilization of aerial photographs is limited by the lack of pre-event and post-event coverage. Although satellite remote sensing has shown potential for hazard/damage assessment (e.g., Mckean *et al.*, 1991; Rengers *et al.*, 1992; Walsh and Butler, 1997), the studies that have used satellite data for hazard/damage assessment of flood and erosion remain limited.

The availability of repeated digital satellite data covering large areas is valuable for quick and efficient mapping. For example, changing response of vegetation in the red and infrared wavelength region (Tucker and Maxwell, 1976; Tucker, 1979; Anderson and Hanson, 1992; Richardson and Everitt, 1992) have provided the opportunity to monitor green vegetation and biomass changes in forest ecosystem (e.g., Chavez and Mackinnon, 1994; Foody and Curran, 1994). Because land cover exhibits abrupt changes in spectral characteristics due to disturbance, digital multitemporal satellite data captured prior to and after heavy rainfall allows the pixel-to-pixel detection analysis of affected areas. Although the basic idea is to detect changes based on change in brightness value (BV) at a particular wavelength, different bands or a variety of change-detection techniques may be applied. Change-detection algorithms are usually influenced by the intended type of change to be detected (e.g., Nelson, 1983; Howarth and Boasson, 1983; Virag and Colwell, 1987; Singh, 1989; Peters *et al.*, 1993; Jacobberger-Jellison, 1994; Cablik *et al.* 1994; Johnson 1994; Leon *et al.*, 1998).

The determination of appropriate bands and the change-detection algorithm that is most suited to solve a particular problem is therefore important. Studies that have used satellite data and evaluated change-detection techniques for the assessments of flood and erosion hazards are limited (Michener and Houhoulis, 1998). The selection of a single change-detection technique to address a specific problem is not easy because land-cover spectral responses to a disturbance may vary markedly by type and intensity of disturbance, ecosystem type, and

A.S. Dhakal is with the Department of Forest Resources Management, University of British Columbia, 2nd Floor, Forest Sciences Centre, 2424 Main Mall, Vancouver, BC V6T 1Z4, Canada (dhakal@interchange.ubc.ca).

T. Amada is with the Institute of Agricultural and Forest Engineering, University of Tsukuba, Tennodai 1-1-1, Tsukuba shi, Ibaraki ken 305-8572, Japan.

M. Aniya is with the Institute of Geoscience, University of Tsukuba, Tennodai 1-1-1, Tsukuba shi, Ibaraki ken, 305-8571, Japan.

R.R. Sharma is with the Forest Survey Division, Department of Forest Research and Survey, P.O. Box 3101, Babarmahal, Kathmandu, Nepal.

Photogrammetric Engineering & Remote Sensing
Vol. 68, No. 3, March 2002, pp. 233–239.

0099-1112/02/6803–233$3.00/0

other environmental factors (Collins and Woodcock, 1996; Michener and Houhoulis, 1998). Determining the appropriate change-detection techniques to solve a particular problem requires investigation and examination of different algorithms in a variety of ecosystems (Cohen *et al.*, 1996; Michener and Houhoulis, 1998).

This study compares different change-detection techniques to detect areas affected by heavy rainfall and compares them using a study site in Nepal, where sediment-related disasters result in an annual average loss of 400 lives and property losses amounting to US $17 million (DPTC, 1994). Analyses of standard accuracy and spatial agreement are performed to compare the new images (hereafter called "change images") representing the change between the two dates. Spatial agreement evaluates the conformity in the classified "change pixels" and "no-change pixels" at the same location on different change images and comprehensively examines the different techniques. The objectives of this study were to use multitemporal Landsat TM data (1) to examine the potential of TM data in detecting areas affected by flood and erosion caused by a heavy rainfall, (2) to perform and evaluate different techniques of change-detection to map areas affected by flood and erosion, and (3) to examine the spatial agreement in the change images produced from different change-detection techniques.

Study Area

The study area is the Kulekhani watershed located in the Lesser Himalayan region of the Himalayan belt in the central region of Nepal. The drainage area of 124 km^2 lies between 27° 34′ N and 27° 42′ N latitude and between 85° 01′ E and 85° 12′ E longitude, with elevation ranging from 1,500 m to 2,600 m (Figure 1). The Lesser Himalayan region in Nepal is highly populated and prone to flash floods, floods, debris flows, and landslides. The average annual rainfall is about 1600 mm. The area is drained by the Palung river, which empties into the Kulekhani reservoir.

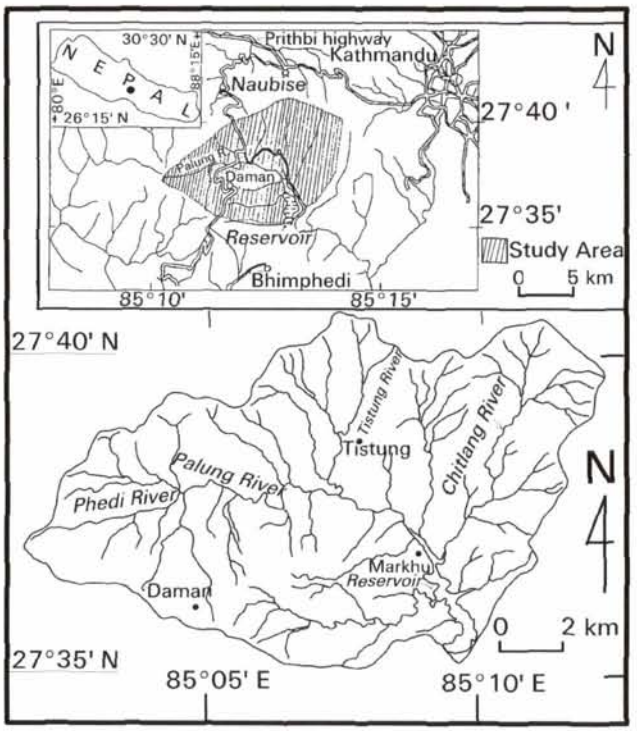

Figure 1. Location of the Kulekhani watershed, Nepal showing general drainage patterns.

Agricultural crops occupy 43 percent of the total land area (Department of Forest, Nepal, 1991). Forest occupies 44 percent of the total land area, in which coniferous, broadleaf, and mixed forests occupy 18 percent, 14 percent, and 12 percent, respectively (Department of Forest, Nepal, 1991). Shrub land, grassland, rock outcrops, and a reservoir cover the remaining 13 percent of the watershed (Department of Forest, Nepal, 1991). The geology of the study area is characterized by sedimentary or weakly metamorphosed rocks consisting of slates, limestones, meta-sandstones, phyllites, schists, quartzites, and granite (Stocklin and Bhattarai, 1981).

The Kulekhani watershed received an average rainfall of 350 mm on 19 July 1993, which caused landslides, debris flows, and floods in many parts of the watershed. Many villages were affected during this erosion disaster, which killed some 72 people and destroyed houses, lands, and infrastructure. The Kulekhani reservoir received 5.9 million m^3 of sediments between March 1993 and December 1993 (Dhakal, 1995).

Methods of Analysis

Pre-Processing of TM Data

Two Landsat TM images dated 20 December 1990 and 29 December 1993 were used for the analysis. The 1990 image depicts the pre-disturbance condition, and that of 1993 depicts the post-disturbance condition during which land use had not changed appreciably. The study area is one of the most conserved areas because of the presence of the only reservoir in Nepal, which supports one-third of the total electric power generation of Nepal. Hence, land-use changes between 1990 and 1993 due to other reasons such as deforestation were unlikely. Similarly, during three field visits between July 1993 and March 1994 any other notable changes in land use due to reasons other than rainfall between July 1993 (event date) and December 1993 (image date) were not encountered.

Thirty-four ground control points (GCPs) digitized from the 1:25,000-scale topographic map were used to rectify the 20 December 1990 Landsat TM image to a Universal Transverse Mercator (UTM) map projection (root-mean-square error: RMSE = 0.46 pixel/14 m). The 1993 image was registered using 50 GCPs obtained from the rectified 1990 image (RMSE = 0.31 pixel/9 m). Both RMSEs are within acceptable limits for change-detection analysis. RMSE errors less than 0.5 pixel in sparsely vegetated areas have been shown to retain very high accuracy (greater than 97 percent) in the change-detection analysis (Townshend *et al.*, 1992). The images were resampled to a 30-m pixel size using the nearest-neighbor resampling technique to retain radiometric integrity (Jensen, 1996).

Empirical scene normalization techniques described by Eckhardt *et al.* (1990) were used in this study to minimize or eliminate the effect of astronomic, atmospheric, and phase angle differences between the 1990 and 1993 TM images. The 1993 TM image was selected as the reference image to which the 1990 image was normalized. The pixel clusters of "normalization targets" (Jensen *et al.*, 1995) were extracted from three wet (reservoir) and six dry (rock outcrops/grassland) areas in both the 1993 and the 1990 images. Normalization targets were assumed to be the constant reflectors, so any changes in their BVs were attributed to astronomic, atmospheric, and phase angle differences (Hall *et al.*, 1991). Regression equations were derived for each band (Table 1). The coefficients and intercept of the equation were used to obtain the normalized 1990 TM image. Once these variations in the multiple-date images were removed, changes in BV could be related to changes in surface conditions.

Response of Different Bands of Landsat TM data

The differences in the BV between the 1993 and 1990 images for some areas affected by heavy rainfall are shown in Figure 2. The information on these areas were collected in the field in a similar manner to reference data collected for accuracy assessment (to

TABLE 1. REGRESSION EQUATIONS USED TO NORMALIZE RADIOMETRIC CHARACTERISTICS OF THE 1990 DATA WITH 1993 DATA

TM Bands	Regression Equation Derived	R^2
Band 1	Y = 1.177X + 1.789	0.989
Band 2	Y = 1.059X + 2.154	0.991
Band 3	Y = 1.241X + 0.904	0.995
Band 4	Y = 1.095X + 1.042	0.998
Band 5	Y = 1.085X + 1.143	0.999
Band 7	Y = 1.154X − 1.192	0.996

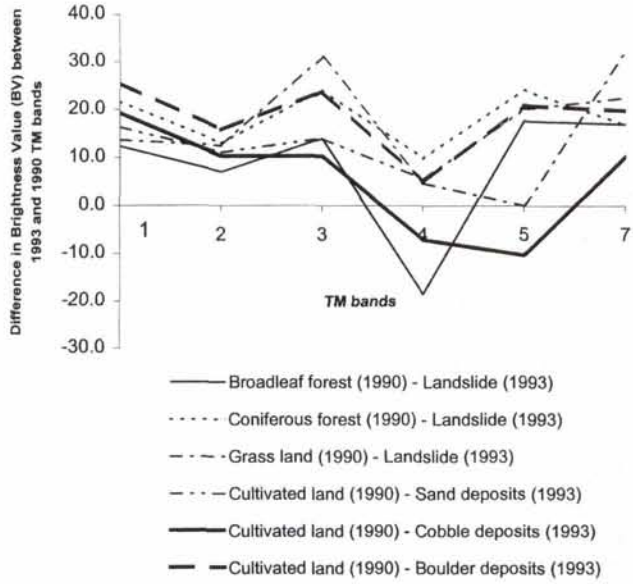

Figure 2. Change in brightness value between 1993 (post-disturbance) and 1990 (pre-disturbance) TM bands for some areas affected by flood and erosion. Values greater than zero indicate increase in brightness value in 1993 image. Legend also depicts the land-use/land-cover types prior to the disturbance.

be discussed later). The mean values for each band were extracted from a 3 by 3 matrix. Bands 1, 2, 3, and 7 display distinct differences in the BV in a variety of affected areas. Bands 4 and 5 display a mixed response. With this information, four different change-detection techniques including Spectral Image Differencing (SID), Tasseled Cap Brightness Image Differencing (TCBID), Principal Component Analysis (PCA), and Spectral Change Vector Analysis (SCVA) were employed. Because bands 4 and 5 were less effective in representing varieties of affected areas occurring for all land uses, SID was performed on the four bands (band 1: blue, band 2: green, band 3: red, and band 7: mid-infrared). SCVA and PCA used three visible bands. Band 7 was excluded because a preliminary analysis by visual inspection suggested better results with the visible bands. Altogether, seven change images were generated using these four techniques.

Spectral Image Differencing (SID)

For the pixel located at row i and column j, the difference in the brightness value (DBV_{ij}^k) for band k between the two dates was computed as (Jensen, 1996)

$$DBV_{ij}^k = BV_{ij}^k(t_2) - BV_{ij}^k(t_1) + C \quad (1)$$

where BV is Brightness value, t_2 is second date (in this case 1993), t_1 is first date (in this case 1990), and C is a constant taken as 127.

Tasseled Cap Brightness Image Differencing (TCBID)

The tasseled cap transformation defines a new coordinate system in which characteristics of the remotely sensed data can be more readily viewed (Kauth and Thomas 1976; Crist 1983; Crist and Cicone, 1984; Crist and Kauth, 1986). Among three functions of tasseled cap transformation—"brightness," "greenness," and "wetness,"—only the brightness function was employed, and was computed as follows (Mather, 1988):

$$\begin{aligned} \text{Brightness} = {} & 0.3037\ (\text{TM1}) + 0.2793\ (\text{TM2}) \\ & + 0.4343\ (\text{TM3}) + 0.5585\ (\text{TM4}) \\ & + 0.5082\ (\text{TM5}) + 0.1863\ (\text{TM7}). \end{aligned} \quad (2)$$

The image showing change in brightness was produced by subtracting the brightness function for 1990 from that of 1993.

Principal Component Analysis (PCA)

The PCA in this study was based on merged data sets of bands 1, 2, and 3 from the images of 1990 and 1993 (Duvernoy and Leger, 1980). The basic premise for the PCA with merged data in change detection is that one or more of the new PCA bands contain information that can be directly related to change (Byrne *et al.*, 1980). Muchoney and Haack (1994) demonstrated that multitemporal SPOT spectral information related to hardwood defoliation by gypsy moths was confined to a single PCA band.

The eigenvalues and eigenvectors of the 6 by 6 covariance matrix of the six-dimensional merged TM data of 1990 and 1993 were computed. The first, second, and third principal components accounted for 96.2 percent, 2.8 percent, and 0.9 percent of the variance, respectively. Analysis of the eigenvector of the transformed data and visual inspection of six images indicated that a third component image best represents the areas affected by flood and erosion. Fung and LeDrew (1987) have shown that the standardized PCA (using correlation matrix) performed better than the unstandardized PCA (using covariance matrix). Our study did not show any significant difference between them; hence, we considered only the unstandardized PCA.

Spectral Change Vector Analysis (SCVA)

When land undergoes a change due to disturbance, the vector describing the direction and magnitude of change from the first to the second date is a spectral change vector (Malila, 1980). The total change in magnitude per pixel (CM_{pixel}) between the dates through n-dimensional change space was computed as (Malila, 1980)

$$CM_{pixel} = \sum_{k=1}^{n} [BV_{i,j,k(date2)} - BV_{i,j,k(date1)}]^2 \quad (3)$$

where $BV_{i,j,k(date2)}$ and $BV_{i,j,k(date1)}$ are the date 1 and date 2 pixel values in band k, respectively.

Three visible bands (band 1: blue, band 2: green, and band 3: red) were selected for SCVA. A scale factor of five was used to process each TM band. The use of three bands provides eight possible types of change vectors (Michalek *et al.*, 1993). Because different affected areas show increments in bands 1, 2, and 3 due to disturbances (see Figure 2), only a change of vector, which resulted from an increase in BV in bands 1, 2, and 3, was of interest.

Thresholding and Accuracy Assessment

Except for the change image produced from SCVA, which has a one-tail histogram, the histograms of other change images show

nearly normal distributions. Figure 3 shows an example of SID (band 1). Values near the mean indicate that they have similar spectral values on both dates, and therefore have experienced no disturbances. The values that are less than or close to the mean (i.e., represented by the left-side tail of the histogram) indicate areas where spectral values decreased in 1993 or remained relatively unchanged. These are the pixels considered unaffected by disturbances because they indicate the annual ephemeral changes in land cover, which are not of interest to us. The area affected by heavy rainfall was represented by pixels belonging to the right-side tail of the histogram.

The following discussion illustrates the method of determining threshold boundaries between change and no-change pixels. Threshold images were produced by adding the standard deviation times N to the mean, with N values equal to 0.25, 0.5, 0.75, 1.0, 1.25, 1.5, 1.75, 2.0, 2.25, and 2.5. Threshold images are binary images in which a value of 0.0 or 1.0 represents no-change or change, respectively. The change images produced at each threshold value were compared with the reference data (discussed in the following paragraph). Overall accuracy and Khat were used for evaluation and determination of the optimal threshold (Congalton *et al.*, 1983; Congalton, 1991). An example of a selection of an optimal threshold for SID (band 1) is shown in Table 2.

The 94 reference data (at least 100 m wide) were collected in the field using a GPS. Of these, 50 are from the affected areas and 44 are from the not-affected areas, in which the sizes of the not-affected areas were relatively larger. The reference sites were so selected that most types of affected areas and not-affected land uses were included. The information on location of reference sites was then brought into a GIS for overlaying with change images and the subsequent accuracy assessment. The reference data finally consisted of 1,468 no-change pixels and 1,075 pixels from the areas affected by the heavy rainfall. Among 1,075 change pixels, 388 pixels represented landslide (slope failure) pixels and the remaining pixels represented sediment deposits located in the alluvial fan and river terraces.

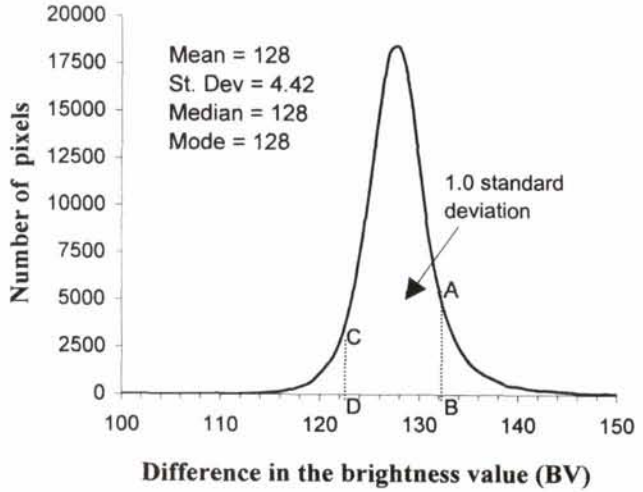

Figure 3. Smoothed histogram of change image produced from Spectral Image Differencing (SID; band 1). Statistics representing characteristics of histogram are also shown, which were used for thresholding and to determine the optimal threshold value. Line AB at right-side tail and CD at left-side tail show boundaries of 1.0 standard deviation values. The area affected by heavy rainfall was represented by pixels belonging to the right side of AB because pixels belonging to the left side of CD represented the annual ephemeral changes in land cover, which were not of interest to us (also see text and Table 2 for the explanation).

TABLE 2. THRESHOLD VALUES CORRESPONDING TO VALUE OF THE STANDARD DEVIATION TIMES N TO THE MEAN (N = 0.25 TO 2.5) FOR SID (BAND 1) CHANGE IMAGE. OVERALL ACCURACY AND THE KHAT DETERMINED THE OPTIMAL THRESHOLD FROM THE RANGE

	Spectral Image Differencing (SID; band 1)		
		Accuracy	
N	Threshold Value	Overall Accuracy	Khat
0.25	129	84.7	69.0
0.50	130	85.5	70.3
0.75	131	86.4	71.7
1.00	132	87.0	72.6
1.25	133	86.1	70.5
1.50	134	85.3	68.7
1.75	135	84.2	66.0
2.00	136	83.0	63.2
2.25	138	80.0	56.3
2.50	139	76.1	47.1

The method for determining the optimal threshold for the change image produced from SCVA is a modification of the method for a normally distributed histogram. Initially, a lower value of spectral change vector magnitude was chosen and then selectively modified to the upper magnitudes until the highest accuracy was achieved.

Results

Table 3 compares the overall accuracy and Khat in change images produced by different change-detection techniques. Among the seven change images, SCVA (using bands 1, 2, and 3) performed best in detecting the affected areas with overall and Khat accuracies of 88.3 percent and 75.4 percent, respectively. Following SCVA were SID (band 2) and PCA with overall accuracies of 87.5 percent and 87.4 percent, respectively, and Khat accuracies of 73.6 percent and 73.4 percent, respectively. SID (band 7) showed poor accuracy compared to the visible bands. Among the visible bands employed for the SID, band 2 showed the highest accuracy followed by bands 1 and 3. TCBID, the weighted average of six TM bands (excluding band 6), showed the least accuracy. Six change images (excluding the SCVA change image) had the optimal threshold at N = 1 at which both overall accuracy and Khat were highest.

The results indicate the effectiveness of visible bands of TM data. Accuracies were improved when all visible bands were used together in the algorithm. Figure 4 shows a change image generated from SCVA at the optimal threshold value along with subsets of post-disturbance aerial photo and TM image (band 2). About 10 percent of the watershed was detected as affected by flood and erosion.

TABLE 3. COMPARISON OF OVERALL ACCURACY (%) AND KHAT (%) FOR DIFFERENT CHANGE DETECTION TECHNIQUES AT THE OPTIMAL THRESHOLD VALUE

Change Detection Method and Band(s) Employed	Overall Accuracy	Khat
Spectral Image Differencing (SID; band 1)	87.0	72.6
Spectral Image Differencing (SID; band 2)	87.5	73.6
Spectral Image Differencing (SID; band 3)	86.0	70.5
Spectral Image Differencing (SID; band 7)	82.9	63.5
Tasseled Cap Brightness Image Differencing (TCBID)	78.7	54.1
Principle Component Analysis (PCA; 3rd component)	87.4	73.4
Spectral Change Vector Analysis; (SCVA; sector which showed BV increase in all bands 1, 2, and 3)	88.3	75.4

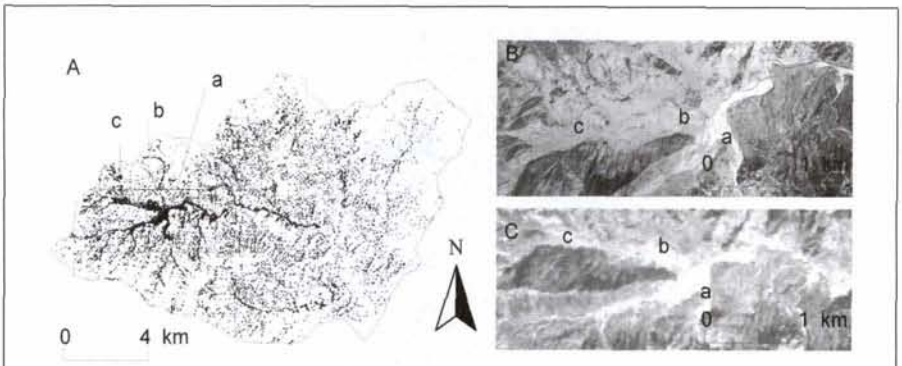

Figure 4. (A) A Map of Kulekhani watershed (see Figure 1) showing areas affected by flood and erosion (black spots) based on the Spectral Change Vector Analysis (SCVA) (e.g., (a) sand deposits in granite area, (b) sand deposits in schist area, (c) cobble deposits in schist area). Subsets of post disturbance (B) 1994 aerial photograph, and (C) December 1993 Landsat TM (Band 2) are also shown.

Evaluation of Spatial Agreement between Change Images

Accuracy assessment is a common method to evaluate change images; however, it does not exactly explain how two change images produced from different techniques differ from each other. Spatial agreements between change images were examined to comprehensively evaluate change images produced from different techniques.

To evaluate spatial agreements between change images, two of the seven change images were overlaid in turn and all the pixels (i.e., "change" and "no-change"), classified into the same category (agreed pixels), were counted. The "overall spatial agreement" was then calculated by taking the proportion of agreed pixels to the total number of pixels, in a similar manner to the evaluation of overall accuracy from the error matrix (e.g., Congalton *et al.*, 1983; Congalton, 1991).

The "overall spatial agreement" in the change images varied from 89 percent to 98 percent (Table 4). The agreement was high among the change images obtained by SID (band 3), PCA, and SCVA. The "overall spatial agreements" were usually higher in all cases due to the influence of a large number of "no-change" pixels (about 90 percent) compared to "change pixels" (about 10 percent). Nevertheless, the "overall spatial agreement" is a good indicator of the similarity between the change images because it reveals the subtle differences between them.

The "overall spatial agreement" measures the agreement of the entire change image. Often, it might be important to compute agreement only among the "change" category. For this reason, the spatial agreement was also computed for the change category. Because the change image produced from SCVA was the most accurate change image, the agreement in the change category for the other six change images was compared with the change image of SCVA. After overlaying six change images with the change image of SCVA, the "spatial agreement in the change category" was calculated as the proportion of "agreed change pixels" to the "total change pixels" (Table 5). For comparison, "spatial agreement in the no-change category" (the proportion of "agreed no-change pixels" to the "total no-change pixels") was also calculated in a similar manner and shown in Table 5. Table 5 shows highest agreement between SCVA and SID (band 3) followed by SCVA and PCA, and SCVA and SID (band 2).

Discussion and Conclusions

Among the individual bands of TM data used, the visible bands were effective in detecting flood and erosion areas. In SID, band 2 shows the highest accuracy (overall accuracy 87.5 percent and Khat 73.6 percent) followed by band 1 (overall accuracy 87.0 percent and Khat 72.6 percent) and band 3 (overall accuracy 86.0 percent and Khat 70.5 percent). A study conducted by Ridd and Liu (1998) showed that band 3 and band 2 were effective in detecting changes at a construction sites and farmlands in an urban environment. Miller *et al.* (1983) and Patel *et al.* (1985) found muddy water showing higher reflectance for band 3 (red). Yamagata and Akiyama (1988) also used band 3 to estimate paddy damage caused by flooding using multitemporal Landsat data. The subtle difference in this study was encountered because the type and size of deposits varied in different affected areas. It is important to note that the change image produced from SCVA, which showed the highest accuracy among different change-detection techniques, had higher spatial agreement with the change image produced from SID (band 3) than the change image produced from SID (band 2) (see Tables 4 and 5).

Among the different change-detection techniques tested, SCVA (using bands 1, 2, and 3) performed best with overall accuracy of 88.3 percent and Khat of 75.4 percent. PCA and SID (bands

TABLE 4. COMPARISON OF OVERALL SPATIAL AGREEMENT (%) BETWEEN SEVEN CHANGE IMAGES PRODUCED FROM DIFFERENT CHANGE-DETECTION TECHNIQUES

	SID (Band 1)	SID (Band 2)	SID (Band 3)	SID (Band 7)	TCBID	PCA	SCVA
SID (Band 1)	100						
SID (Band 2)	93.0	100					
SID (Band 3)	92.5	95.0	100				
SID (Band 7)	89.4	90.8	91.0	100			
TCBID	91.5	93.2	93.3	93.9	100		
PCA	94.8	92.8	97.1	91.1	93.7	100	
SCVA	95.2	96.0	97.5	90.9	93.3	98.1	100

SID: Spectral Image Differencing; TCBID: Tasseled Cap Brightness Image Differencing; PCA: Principle Component Analysis (3rd component); SCVA: Spectral Change Vector Analysis (vector which showed BV increase in all bands 1, 2, and 3).

TABLE 5. SPATIAL AGREEMENT OF CHANGE AND NO-CHANGE CATEGORY (%) OF SIX CHANGE IMAGES COMPARED AGAINST THAT OF CHANGE IMAGE PRODUCED FROM SPECTRAL CHANGE VECTOR ANALYSIS (SCVA)

Change detection method	Change category	No-change category
SID (Band 1)	72.4	98.2
SID (Band 2)	76.8	98.5
SID (Band 3)	88.1	98.7
SID (Band 7)	59.0	95.2
TCBID	68.9	96.9
PCA	85.2	99.8

SID: Spectral Image Differencing; TCBID: Tasseled Cap Transformation Brightness Image Differencing; PCA: Principle Component Analysis (3rd component).

1, 2, and 3) also showed high accuracies. SID (band 7) and TCBID did not perform well. The change image produced from SCVA showed overall spatial agreements of 98.1, 97.5, and 96.0 percent with the change images produced from PCA, SID (band 3), and SID (band 2), respectively. SCVA and SID (band 3) showed the spatial agreement of 88.1 percent and 98.7 percent with the change and no-change categories, respectively. The rock types of sediments and the type of land cover influenced the change-detection techniques. For example, SID (band 7) and TCBID failed to satisfactorily detect the cobble-type debris flow deposits on cultivated land around the Phedi River in schists and quartzites areas; however, both techniques detected sand deposits on river terraces in granitic areas (see Figures 1 and 4).

SID and TCBID applied in this study were image differencing. Image differencing is a relatively simple and easy technique. Despite its simplicity, SID has been found effective in many studies (e.g., Ridd and Liew, 1998; Macleod and Congalton, 1998; Muchoney and Haack, 1994). The other two techniques—SCVA and PCA—employ many bands together in order to extract changes. These methods have also been found useful in different change-detection studies (e.g., Michalek *et al.*, 1993; Lambin and Strahler, 1994a; Lambin and Strahler, 1994b; Muchoney and Haack, 1994; Yamagata and Akiyama, 1988; Fung and LeDrew, 1987). Due to hydrologic processes, flood and erosion hazard assessment related studies need to be carried out in a watershed usually consisting of different land uses. It is important that change-detection techniques should address the changes occurring in a variety of land uses. Change-detection techniques may be influenced by types of erosion and sedimentation conditions in different land uses.

The application of multitemporal Landsat TM data to detect areas affected by floods and erosion in a watershed consisting of different land uses showed that visible bands were effective in detecting affected areas. Spectral Change Vector Analysis (SCVA; using bands 1, 2, and 3) performed the best followed by Spectral Image Differencing (SID; band 2) and Principal Component Analysis (PCA; using bands 1, 2, and 3). Because the detection of areas affected by flood and erosion in a large area based on fieldwork is often a difficult task, the results of this study enhance the understanding of the practical applicability of automated change detection using multitemporal satellite data in overcoming such difficulties.

Acknowledgments

The work reported in this paper was carried out while the principal author was a graduate student at the University of Tsukuba, Japan. The study was supported by the Department of Forest Research and Survey, Nepal and Water-Induced Disaster Prevention Technical Centre, Nepal. The authors gratefully acknowledge John Innes (Professor, University of British Columbia, Canada) and Younes Alila (Assistant Professor, University of British Columbia, Canada) for their valuable comments on the manuscript. The suggestions made by three anonymous reviewers are highly appreciated. The work is dedicated to the victims of the flood and erosion disaster of 1993 in Nepal.

References

Anderson, G., and J. Hanson, 1992. Evaluating hand-held radiometer derived vegetation indices for estimating above ground biomass, *Geocarto International*, 1:71–77.

Aniya, M., M. Etaya, and H. Shimoda, 1985. Evaluation of Landsat data for landslide identification as a means for watershed management, *Journal of the Japan Society of Photogrammetry and Remote Sensing*, 24(4):17–21.

Brabb, E.E., 1991. The world landslide problem, *Episodes*, 14(1):52–61.

Byrne, G.F., P.F. Crapper, and K.K. Mayo, 1980. Monitoring land-cover change by principal component analysis of multitemporal Landsat data, *Remote Sensing of Environment*, 10:175–184.

Cablik, M.E., B. Kjerfve, W.K. Michener, and J.R. Jensen, 1994. Impacts of Hurricane Hugo on a coastal forest: Assessment using Landsat TM data, *Geocarto International*, 2:15–24.

Carrara, A., M. Cardinali, R. Detti, and F. Guzzetti, 1992. Uncertainty in assessing landslide hazard and risk, *ITC Journal*, 2:172–183.

Carrara, A., M. Cardinali, R. Detti, F. Guzzetti, and P. Reichenbach, 1995. *GIS technology in mapping landslide hazard*, Geographical Information Systems in Assessing Natural Hazards (A. Carrara and F. Guzzetti, editors), Kluwer Academic Publishers, Dordrecht, The Netherlands, pp. 135–175.

Chavez, P.S., and D.J. Mackinnon, 1994. Automatic detection of vegetation changes in the southwestern U.S. using remotely sensed images, *Photogrammetric Engineering & Remote Sensing*, 60(5): 571–583.

Cohen, W.B., J.D. Khusla, W.J. Ripple, and S.L. Garman, 1996. An introduction to digital methods in remote sensing of forested ecosystems: Focus on the Pacific North West, USA, *Environmental Management*, 20(3):421–435.

Collins, J.B., and C.E. Woodcook, 1996. An assessment of several linear change detection techniques for mapping forest mortality using multitemporal Landsat TM data, *Remote Sensing of Environment*, 56:66–77.

Congalton, R.G., 1991. A review of assessing the accuracy of classifications of remotely sensed data, *Remote Sensing of Environment*, 37:35–46.

Congalton, R.G., R.G. Oderwald, and R.A. Mead, 1983. Assessing Landsat classification accuracy using discrete multivariate statistical techniques, *Photogrammetric Engineering & Remote Sensing*, 49(12):1671–1678.

Crist, E.P., 1983. The thematic mapper tasseled cap-a preliminary formulation, *Proceedings of Machine Processing of Remotely Sensed Data*, 21–23 June, West Lafayette, Indiana, pp. 357–363.

Crist, E.P., and R.C. Cicone, 1984. Application of the tasseled cap concept to simulated thematic mapper data, *Photogrammetric Engineering & Remote Sensing*, 50(3):343–352.

Crist, E.P., and R.J. Kauth, 1986. The tasseled cap de-mistyfied, *Photogrammetric Engineering & Remote Sensing*, 52(1):81–86.

Cuny, F.C., 1983. *Disaster and Development*, Oxford University Press, New York, N.Y., 277 p.

Department of Forest, Nepal, 1991. *Land Use Map of Kulekhani Watershed* (1:25,000), Finnish International Dev. Agency (FINNIDA)/ Department of Forest, 1 sheet.

Dhakal, A.S., 1995. Disaster of 1993 experienced by Nepal, *Proceedings of the International Sabo Symposium*, 28–30 August, Tokyo, Japan, pp. 115–122.

Dhakal, A.S., T. Amada, and M. Aniya, 1999. Landslide hazard mapping and the application of GIS in the Kulekhani watershed Nepal, *Mountain Research and Development*, 19(1):3–16.

———, 2000. Landslide hazard mapping and its evaluation using GIS: An investigation of sampling scheme for grid-cell based quantitative method, *Photogrammetric Engineering & Remote Sensing*, 66(8):981–990.

Disaster Prevention Technical Center (DPTC), 1994. *Annual Disaster Review 1993*, Water Induced Disaster Prevention Technical Center, Lalitpur, Nepal, 90 p.

Duvernoy, J., and J. Leger, 1980. Karhunen-Loeve analysis of multispectral data from Landscapes, *Optics Communications*, 32(1):39–44.

Eckhardt, D.W., J.P. Verdin, and G.R. Lyford, 1990. Automated update of an irrigated lands GIS using SPOT HRV imagery, *Photogrammetric Engineering & Remote Sensing*, 56(11):1515–1522.

Foody, G.M., and P.J. Curran, 1994. Estimation of tropical forest extent and regenerative stage using remotely sensed data, *Journal of Biogeography*, 21:223–244.

Fookes, P.G., S.G. Dale, and J.M. Land, 1991. Some observations on a comparative aerial photography interpretation of a landslipped area, *Quartenary Journal of Engineering Geology*, 24:249–265.

Fung, T., and E. LeDrew, 1987. Application of principal components analysis to change detection, *Photogrammetric Engineering & Remote Sensing*, 53(12):1649–1658.

Hall, F.G., D.E. Strebel, J.E. Nickeson, and S.J. Geetz, 1991. Radiometric reflection: Toward a common radiometric response among multidate multisensor images, *Remote Sensing of Environment*, 35: 11–27.

Howarth, P.J., and E. Boasson,1983. Landsat digital enhancements for change detection in urban environments, *Remote Sensing of Environment*, 13:149–160.

ICIMOD, 1991. *Risk Engineering in the Hindu Kush-Himalaya*, International Centre for Integrated Mountain Development (ICIMOD), Kathmandu, Nepal, 106 p.

Jacobberger-Jellison, P.A., 1994. Detection of post drought environmental conditions in the Tombouctou region, *International Journal of Remote Sensing*, 15(16):3138–3197.

Jensen, J.R., 1996. *Introductory Digital Image Processing*, Prentice-Hall, Englewood Cliffs, New Jersey, 316 p.

Jensen, J.R., K. Rutchey, M.S. Kouch, and S. Narumalani, 1995. Inland wetland change detection in the Everglades water conservation area 2A using a time series of normalized remotely sensed data, *Photogrammetric Engineering & Remote Sensing*, 61(2):199–209.

Johnson, R.D., 1994. Change vector analysis for disaster assessment: A case study of Hurricane Andrew, *Geocarto International*, 1:41–45.

Kauth, R.J., and G.S. Thomas, 1976. The tasseled cap-a graphic description of the spectral-temporal development of agricultural crops seen by Landsat, *Proceedings of Machine Processing of Remotely Sensed Data*, 29 June–01 July, West Lafayette, Indiana, Section 4B, pp. 41–51.

Kienholz, H., G. Schneider, M. Bichsel, M. Grunder, and P. Mool, 1984. Mapping of mountain hazards and slope stability, *Mountain Research and Development*, 4(3):247–266.

Lambin, E.F., and A.H. Strahler, 1994a. Change-vector analysis in multitemporal space: A tool to detect and categorize land-cover change processes using high temporal-resolution satellite data, *Remote Sensing of Environmet*, 48:231–244.

———, 1994b. Indicators of land-cover change for change-vector analysis in multitemporal space at coarse spatial scales, *International Journal of Remote Sensing*, 15(10):2099–2119.

Leon, J.G., D. Yuan, R.S. Lunetta, and C.D. Elvidge, 1998. A change detection experiment using vegetation indices, *Photogrammetric Engineering & Remote Sensing*, 64(2):143–150.

Macleod, R.D., and R.G. Congaton, 1998. A quantitative comparison of change detection algorithms for monitoring eelgrass from remotely sensed data, *Photogrammetric Engineering & Remote Sensing*, 64(3):207–216.

Malila, W.A., 1980. Change vector analysis: An approach for detecting forest changes with Landsat, *Proceedings of the LARS Machine Processing of Remotely Sensed Data Symposium*, 03–06 June, West Lafayette, Indiana, pp. 326–336.

Mantovani, F., R. Soeters, and C.J. Van Westen, 1996. Remote sensing techniques for landslide studies and hazard zonation in Europe, *Geomorphology*, 15:213–225.

Mather, P.M. 1986. *Computer Processing of Remotely Sensed Images*, John Wiley & Sons, New York, N.Y., 353 p.

McKean, J., S. Buechel, and L. Gaydos, 1991. Remote sensing and landslide hazard assessment, *Photogrammetric Engineering & Remote Sensing*, 57(9):1185–1193.

Michalek, J.L., T.W. Wagner, J.J. Luczkovich, and R.W. Stoffle, 1993. Multispectral change vector analysis for monitoring coastal marine environments, *Photogrammetric Engineering & Remote Sensing*, 59(3):381–384.

Michener, W.K., and P.F. Houhoulis, 1998. Detection of vegetation changes associated with extensive flooding in a forested ecosystem, *Photogrammetric Engineering & Remote Sensing*, 63:1363–1374.

Miller, L.D., Y. Yang, M. Matthews, and R.T. Irons, 1983. Correlations of rice yields to radiometric estimates of canopy biomass as a function of growth stage, *Proceedings of the Fourth Asian Conference of the Remote Sensing*, 10–15 November, Colombo, Sri Lanka, A.6.1–A.6.21

Muchoney, D.M., and B.N. Haack, 1994. Change detection for monitoring forest defoliation, *Photogrammetric Engineering & Remote Sensing*, 60(10):1243–1251.

Nelson, R.F., 1983. Detecting forest canopy change due to insect activity using Landsat MSS, *Photogrammetric Engineering & Remote Sensing*, 49(9):1303–1314.

Patel, N.K., T.P. Singh, B. Sahai, and M. Patel, 1985. Spectral response of rice crops and its relation to yield and yield attributes, *Internation Journal of Remote Sensing*, 6:657–664.

Peters, A.J., B.C. Reed, M.D. Eve, and K.M. Havstad, 1993. Satellite assessment of drought impact on native plant communities of southeastern New Mexico, U.S.A., *Journal of Arid Environments*, 24:305–319.

Rengers, N.R., R. Soeters, and C.J. Van Westen, 1992. Remote sensing and GIS applied to mountain hazard mapping, *Episodes*, 15(1):36–45.

Richardson, A.J., and J.H. Everitt, 1992. Using spectral vegetation indices to estimate rangeland productivity, *Geocarto International*, 1:63–69.

Ridd, M.K., and J. Liu, 1998. A comparison of four algorithms for change detection in an urban environment, *Remote Sensing of Environment*, 63:95–100.

Sakai, T., H. Nishikawa, S. Fukuyama, and T. Sugimura, 1985. A study of landslides in Hayakawa watershed by using landsat MSS data - Detection of new landslides, *Journal of the Remote Sensing Society of Japan*, 5:5–15 (in Japanese with English abstract).

Singh, A., 1989. Digital change detection techniques using remotely-sensed data, *International Journal of Remote Sensing*, 10(6): 989–1003.

Stocklin, J., and K.D. Bhattarai, 1981. *Geology of Kathmandu Area and Central Mahabharat Range, Nepal Himalaya*, United Nations Mineral Exploration Technical Report, UNDP/Nepal, 61 p.

Townshend, J.R.G., C.O. Justice, C. Gurney, and J. McManus, 1992. The impact of misregistration on change detection, *The Transactions of Geoscience and Remote Sensing*, 30(5):1054–1060.

Tucker, C.J., 1979. Red and photographic infrared linear combinations for monitoring vegetation, *Remote Sensing of Environment*, 8(2): 127–150.

Tucker, C.J., and E.L. Maxwell, 1976. Sensor design for monitoring vegetation canopies, *Photogrammetric Engineering & Remote Sensing*, 42(11):1399–1410.

Van Westen, C.J., 1993. *Application of Geographic Information System to Landslide Hazard Zonation*, ITC Publication Number 15, Part 1, ITC, Enschede, The Netherlands, 245 p.

Virag, L.A., and J.E. Colwell, 1987. An improved procedure for analysis of change in thematic mapper image-pairs, *Proceedings of the Twenty-First International Symposium on Remote Sensing Environment*, 26–30 October, Ann Arbor, Michigan, pp. 1101–1110.

Walsh, S.J., and D.R. Butler, 1997. Morphometric and multispectral image analysis of debris flows for natural hazard assessment, *Geocarto International*, 12(1):59–70.

Yamagata, Y., and T. Akiyama, 1988. Flood damage analysis using multitemporal Landsat TM data, *International Journal of Remote Sensing*, 9(3):503–514.

Zhou, G., J. Luo, C. Yang, B. Li, and S. Wang, 2000. Flood monitoring using multi-temporal AVHRR and RADARSAT imagery, *Photogrammetric Engineering & Remote Sensing*, 66(5):633–638.

(Received 06 November 2000; accepted 27 April 2001; revised 13 August 2001)